Nonlinear Soil Behavior Examined on the Basis of Propagation Time Observed at the KiK-net Ichinoseki-Nishi Vertical Array

HIDENORI MOGI [*], SHRESTHA SANTA MAN [†], HIDEJI KAWAKAMI[‡] and JUN'YA KAWAMURA[§]

[*] Department of Civil and Environmental Engineering, Saitama University, Japan.

[†] Department of Civil Engineering, Acme Engineering College, Nepal.

[‡] Geosphere Research Institute, Saitama University, Japan.

[§] Saitama City Government, Japan.

Abstract

The Iwate-Miyagi Nairiku earthquake (14 June 2008, *M*7.2, Depth 8 km) caused severe damage in the southern part of Iwate and northern part of Miyagi Prefectures in Japan. The KiK-net Ichinoseki-Nishi vertical array site (IWTH25), operated by the National Research Institute for Earth Science and Disaster Prevention, is situated near the epicenter. The observed peak ground accelerations at the surface in the up-down, east-west, and north-south directions were respectively 3,866 cm/s^2, 1,432 cm/s^2, and 1,143 cm/s^2. The extreme ground motions recorded at this site provide valuable information about the wave propagation and soil degradation at a large strain level.

We examined the nonlinear soil behavior at the site due to the earthquake on the basis of normalized input-output minimization (NIOM) analysis. First, we analyzed 279 records observed before the Iwate-Miyagi Nairiku earthquake and estimated the vertical propagation time (initial value) between the bottom of the well and the ground surface by taking into account incidence angles. Then, we analyzed the records of the Iwate-Miyagi Nairiku earthquake and 179 events that occurred after it (from 14 June 2008 to 19 October 2009). The results revealed that (1) the S-wave propagation time increased from 0.265 s to about 0.35 s because of the nonlinear behavior of the soil; (2) this propagation time

change corresponded to a 60% reduction in the shear moduli of the upper soil layers (ground level–64 m in depth) and a strain level of 1×10^{-3}; (3) a gradual decrease in the propagation time with decreasing seismic intensity was observed soon after the principal motions; however, (4) the propagation times in the coda part and for the events after the Iwate-Miyagi Nairiku earthquake were still larger than the initial value, indicating that the shear rigidities of soils remained less than their values before the earthquake for more than a year.

Introduction

The Iwate-Miyagi Nairiku earthquake (14 June 2008, *M*7.2, Depth 8 km) (e.g., NIED, 2008) caused severe damage in the southern part of Iwate and northern part of Miyagi Prefectures in Japan. The KiK-net Ichinoseki-Nishi vertical array site (IWTH25), operated by the National Research Institute for Earth Science and Disaster Prevention (NIED), is situated near the epicenter (epicentral distance was 3 km). The extreme ground shaking recorded during the mainshock has been discussed especially in regard to the asymmetric vertical acceleration—the upward peak acceleration was 3,866 cm/s^2, whereas the downward value was 1,703 cm/s^2—observed at the ground surface (NIED, 2008; Aoi et al., 2008; Yamada et al., 2009; Ohmachi et al., 2011).

The KiK-net vertical array site is equipped with two sets of accelerometers, one set at the ground surface and the other at the bottom of the well (GL-260 m). The vertical array records provide valuable information about wave propagation and soil degradation at a large strain level.

Various laboratory tests have been conducted by many researchers on soil degradation of different soil types (e.g., Seed and Idriss, 1970; Hardin and Drnevich, 1972a; Hardin and Drnevich, 1972b; Sun et al., 1988), and these studies have revealed

that soil properties are affected by various factors such as shear-strain level, confining stress, and so on. Furthermore, undisturbed specimens have been used in laboratory tests in order to examine the in-situ properties of soils (e.g., Katayama et al., 1986; Hatanaka et al., 1988). However, sampling undisturbed specimens requires significant effort and cannot be used commonly.

Inversion calculations using vertical array records of actual earthquakes have been conducted for the in-situ examination of the nonlinear properties of soil. Satoh et al. (2001) conducted inversion analyses on the vertical array records observed during the 1995 Hyogoken-Nanbu earthquake and found significant soil degradation at Port Island. Satoh (2006) also conducted an inversion analysis of the KiK-net array records in order to evaluate frequency-dependent Qs, S-wave velocity, P-wave velocity, and incidence angles. In the study, a need to take into account the incidence angles of the seismic waves was pointed out. Pavlenko and Irikura (2002 and 2006) used inversion analyses to obtain nonlinear time-dependent stress-strain relations in soil layers from various vertical array records. Tokimatsu et al. (2008) and Tokimatsu and Arai (2008) conducted an inversion analysis of vertical array records observed at the Kashiwazaki-Kariwa Nuclear Power Plant and found a significant reduction in the shear moduli in the Holocene and

Pleistocene sand layers during the 2007 Niigata-ken Chuetsu-oki earthquake. This brief review of previous studies shows that the analysis of vertical array records is an effective means to assess nonlinear soil properties.

Kawakami and Bidon (1997), Kawakami and Haddadi (1998), and Haddadi and Kawakami (1998a) developed the simplified input output relation method (SIORM) and normalized input-output minimization (NIOM) method as ways to examine wave propagation using vertical array records. Application of SIORM to actual vertical array records of Minamisuna and Etchujima sites in Japan revealed clear arrival times for the incident S-wave and reflected S-wave from the surface (Kawakami and Bidon, 1997). NIOM analysis was also applied to the records of the Chiba vertical array in Japan as well as Etchujima and Minamisuna vertical arrays, and it yielded clear arrival times for the incident and reflected S-waves (Kawakami and Haddadi, 1998; and Haddadi and Kawakami 1998a). These results were consistent with the theoretical time arrival of the S-wave obtained from their soil profiles. The NIOM analysis of the 1995 Hyogoken-Nanbu earthquake using records from the Port Island vertical array site clearly showed liquefaction of the surface layer through a decrease in S-wave velocity in the top layer (Hadaddi and Kawakami, 1998b). A NIOM analysis was also conducted on

records of the mainshock and aftershocks of the 2007 Niigata-ken Chuetsu-oki earthquake observed at the vertical array at the Kashiwazaki-Kariwa Nuclear Power Plant (Mogi et al., 2010). The results revealed that the temporal variation of S-wave velocities in the surface layer (surface to 50 m depth) and intermediate layer (50–100 m depth) was observed during the principal motions of the mainshock and the healing process that restored the rigidity of the soils soon after the principal motion.

In this study, we performed a NIOM analysis to assess nonlinear soil behavior due to the extreme ground motion at the KiK-net Ichinoseki-Nishi site during the Iwate-Miyagi Nairiku earthquake. First, we analyzed 279 records observed before the Iwate-Miyagi Nairiku earthquake and estimated the vertical propagation time (the initial value) by taking into account incidence angles. Then, we analyzed the records of the mainshock of the Iwate-Miyagi Nairiku earthquake and 179 events that occurred after it (from 14 June 2008 to 19 October 2009). The results revealed that (1) the S-wave propagation time increased from 0.265 s to about 0.35 s because of the nonlinear behavior of the soil; (2) this change in propagation time corresponded to a 60% reduction in the shear moduli of the upper soil layers (ground level–64 m in depth) at a strain level of 1×10^{-3}, which was estimated from the observed velocity amplitude and S-wave velocity;

(3) a gradual decrease in propagation time with decreasing seismic intensity was observed soon after the principal motions; however, (4) the propagation times in the coda part and for the events after the Iwate-Miyagi Nairiku earthquake were still larger than the initial value, indicating that the shear rigidities of the soils remained less than their values before the earthquake for more than a year.

Outline of the NIOM method

This section outlines the NIOM method that was developed by Kawakami and Haddadi (1998).

The input-output system can be related by means of a transfer function $H(\omega)$. In the frequency domain, the output $G(\omega)$ is given by

$$G(\omega) = H(\omega)F(\omega), \tag{1}$$

where $F(\omega)$ and $G(\omega)$ are the Fourier transforms of the input $f(t)$ and the output $g(t)$.

Since the transfer function solely depends upon the physical characteristics of the system, we can assume that the same transfer function satisfies the relationship

between input and output models. So we can write

$$Y(\omega) = H(\omega)X(\omega), \tag{2}$$

where $X(\omega)$ and $Y(\omega)$ are the Fourier transforms of the input and output models $x(t)$ and $y(t)$, respectively.

The inverse Fourier transform of input model $X(\omega)$ can be written as

$$x(m\Delta t) = \frac{1}{N\Delta t}\sum_{i=0}^{N-1} X(\omega_i)\exp\left(j\frac{2\pi i m}{N}\right). \tag{3}$$

At $t = 0$, i.e., $m = 0$, the amplitude of the input model, $x(0)$, is normalized to unity; then equation (3) becomes

$$\frac{1}{N\Delta t}\sum_{i=0}^{N-1} X(\omega_i) = 1. \tag{4}$$

To get the simplified input and output models, the sum of the squared Fourier amplitude and its time derivatives are minimized subject to the above constraint. Thus, the Lagrange multiplier method gives

$$L = \sum_{i=0}^{N-1}\left[c_X|X(\omega_i)|^2 + k_X\omega_i^2|X(\omega_i)|^2 + c_Y|Y(\omega_i)|^2 + k_Y\omega_i^2|Y(\omega_i)|^2\right] - \lambda\left\{\frac{1}{N\Delta t}\sum_{i=0}^{N-1} X(\omega_i) - 1\right\}, \tag{5}$$

where λ is the Lagrange multiplier, c_X and c_Y are the weighting constants for the corresponding squared Fourier amplitude, and k_X and k_Y are the weighting constants

for its time derivatives. Because the weighting constants are used in the constraint, a larger value of c_X, for example, flattens the input model to a larger extent than the output model. In this study, we simplified the input and output models to the same extent by setting c_X and c_Y to unity. We also used the same values of weighting constants k_X and k_Y:

$$k = k_X = k_Y = 0.0001 \quad (\mathrm{s}^2). \tag{6}$$

Because the weighting constant k is for the time derivatives of the input and output models, increasing the value of k decreases the contribution of the high-frequency components and gives smoother input and output models.

Substituting equations (2) and (6) into equation (5) and minimizing the equation yields

$$\frac{\partial L}{\partial \lambda} = \frac{\partial L}{\partial X(\omega_i)} = \frac{\partial L}{\partial X^*(\omega_i)} = 0, \qquad (i = 0, \ldots, N-1), \tag{7}$$

where * denotes the complex conjugate.

After minimization, the input model $X(\omega_i)$ and output model $Y(\omega_i)$ are obtained as follows:

$$X(\omega_i) = N\Delta t \frac{\dfrac{1}{\left(1 + \dfrac{k_X}{c_X}\omega_i^2\right)\left(c_X + c_Y|H(\omega_i)|^2\right)}}{\displaystyle\sum_{n=0}^{N-1} \frac{1}{\left(1 + \dfrac{k_X}{c_X}\omega_n^2\right)\left(c_X + c_Y|H(\omega_n)|^2\right)}}, \qquad Y(\omega_i) = H(\omega_i)X(\omega_i). \tag{8}$$

Lastly, the inverse Fourier transforms of the input model $X(\omega)$ and output model $Y(\omega)$ give a simplified input model $x(t)$ and $y(t)$ in the time domain. For the calculation of the inverse Fourier transform using FFT, the first half of the Fourier components of the models were calculated using equation (8), and the number of Fourier components was increased by a factor of 16 by padding trailing zeros in order to interpolate time intervals by 1/16. The latter half of the Fourier components were then set to the complex conjugates of the first half to get real-valued waveforms by using the FFT.

As mentioned above, the NIOM method is a simple input-output analysis technique in which the transfer function is calculated from two observation data satisfying the constraint. It is similar to a receiver function (Langston, 1979). In a receiver function, the input $x(t)$ should be a suitable pulse; however, in the NIOM method, adjustment features are included in order to get simplified input and output waveforms.

Observation Site and Analyzed Accelerograms

The KiK-net Ichinoseki-Nishi vertical array site

The KiK-net Ichinoseki-Nishi vertical array (IWTH25) consists of two observation points, one at the ground surface and the other at the bottom of the well (GL-260 m). The soil profile and propagation times of P and S waves assuming vertically propagating waves at the site are shown in Figure 1. The site is on a river terrace in a mountainous region. The soil from the ground surface to a depth of 64 m consists of relatively soft deposits and shows a strong impedance contrast to the underlying sedimentary rock layers.

Figure 2 shows accelerograms recorded during the 14 June 2008 Iwate-Miyagi Nairiku earthquake (a) at the ground surface and (b) at the bottom of the well (GL-260 m). The time interval and the total length of the records are respectively 0.01 s and 300 s (The time interval of the records before 26 Nov 2005 is 0.005 s). The peak ground accelerations at the surface in the up-down, east-west, and north-south directions were respectively 3,866 cm/s^2, 1,432 cm/s^2, and 1,143 cm/s^2, and those at the bottom were 681 cm/s^2, 748 cm/s^2, and 1,036 cm/s^2, respectively. These extremely strong ground motions have been discussed by Aoi et al. (2008), Yamada et al. (2009), and Ohmachi

et al. (2011), and so on, especially with regard to their asymmetric aspect—the upward peak acceleration was 3,866 cm/s^2, whereas the downward value was 1,703 cm/s^2—at the ground surface.

Choice of earthquakes to be analyzed

Because the borehole at the KiK-net Ichinoseki-Nishi site reached a hard rock layer (Vs=1,810 m/s), oblique incidence occurs at the bottom and affects the propagation time from the bottom to the surface. To take this effect into account, we examined the incidence angles of the direct S waves that cause the principal motion in the waveform.

For simplicity, we conducted a two-dimensional wave analysis with an SH line source. Figure 3 shows the horizontally layered velocity model consisting of 54 layers used in this study. This ground model is based on the one used in the source determination analysis of the events in the Tohoku region by Hasegawa et al. (1978). The layer thickness of the crust (from the surface to a 30-km depth) is 2 km (15 layers), and that of the upper part of the mantle (from 30 km to 100 km) is 5 km. For layers deeper than 100 km, larger thicknesses ranging from 10 km to 20 km were used to reduce computations.

Examples of the estimated waveforms are shown in Figure 3b. In this diagram,

the thin lines show the total responses at the surface to the SH line source estimated by the discrete wavenumber method (Bouchon and Aki, 1977) using the propagator matrix technique (Haskell, 1953), whereas the thick lines show the responses only due to the direct S waves estimated by the Cagniard-de Hoop method (Aki and Richards, 1980).

The results for shallow and deep sources for the epicentral distance of L=20 km reveal that the principal motions in the surface response are due to the direct S wave. The surface response for the deeper source at D=40 km has a more complicated waveform for the longer epicentral distance (L=200 km) than the shorter one (L=20 km); however, the direct S wave is the dominant phase at both distances. On the other hand, the result for the shallow and distant source (D=20 km and L=200 km) shows that the direct S wave no longer dominates the waveform. To examine this phenomenon, surface responses due to seismic waves propagating along other three paths are also shown in the diagram. Paths 1 to 3 stand for the refracted waves generated at the Moho interface, the reflected waves at the interfaces in the crust, and the waves reflected at the ground surface then reflected at the interfaces in the crust, respectively. These results shows that the first phase in the total response is due to the refracted waves, and the direct S phase does not dominate due to the destructive interference with the reflected waves. The destructive interference depends on

the source time function; however, it can be seen that the phase due to the waves reflected at the surface (path 3) dominates over other phases.

Considering this phenomenon, we first chose all records of events occurred within 300 km from the Ichinoseki-Nishi site and performed the above-described theoretical calculations for all hypocenter locations. After that, we chose events whose direct S waves dominated the calculated waveforms. The incidence angles of the direct S waves were obtained from the ray parameter at the point of departure of the Cagniard path from the real axis (e.g., Aki and Richards, 1980).

Epicenter map of the analyzed events

Figure 4 shows the epicenters of the 279 analyzed events before the Iwate-Miyagi Nairiku earthquake. The triangular symbol in the map shows the Ichinoseki-Nishi site. Among these events, two major inland earthquakes are included —the 26 May 2003 Sanriku-Minami earthquake (M7.0, Depth 71 km) and the 26 July 2003 Miyagiken-Hokubu earthquake (M6.2, Depth 12 km). Their epicentral distances from the Ichinoseki-Nishi site are 74 km and 72 km, respectively.

Figure 5 shows the epicenters of the Iwate-Miyagi Nairiku earthquake and

analyzed events after it until 19 October 2009. Unfortunately, the event on 19 October 2009 was the last one because the observations at the site ceased after that. The total number of these events is 180, and most of them are the aftershocks of the Iwate-Miyagi Nairiku earthquake. The map also shows a 40 km $\times$ 20 km fault plane with a dip angle of 40 degrees proposed by Suzuki et al. (2010). The depth of the upper edge of the fault was estimated to be 0.7 km. The Ichinoseki-Nishi site is situated just above the center of the fault plane.

NIOM Analysis and Results

Results of NIOM analysis

We used acceleration records for the NIOM analysis in this study. The NIOM analysis for the earthquakes before the Iwate-Miyagi Nairiku earthquake used 10.0-s intervals of the principal motion of the S-wave part, whereas the time intervals for events after it were 4.0 s because most of these subsequent earthquakes were small events near the site, and a 4-s time interval is long enough to cover the duration of the major S-wave part. In the analysis of the mainshock of the Iwate-Miyagi Nairiku earthquake and the

Sanriku-Minami earthquake, a moving window of 4.0-s duration with a cosine taper of 0.25-s intervals on both sides was used from the arrival of the S-wave to 300 s in 2-s increment.

Figure 6 shows some of the results of the analysis. In these results, the values of k_X and k_Y (in equation 6) were 0.0001 s^2; however, the choices of these values are not critical because the peak time in the output model is not affected much by the values. Figure 6a shows the results for the event before the Iwate-Miyagi Nairiku earthquake and Figure 6b shows those for the Sanriku-Minami earthquake. Figures 6c–6f are for the principal motion (the applied time window is 20–24 s) and the coda parts (the time windows of 84–88 s, 186–190 s, and 278–282 s, respectively) of the Iwate-Miyagi Nairiku earthquake. Figures 6g and 6h are for the events after the Iwate-Miyagi Nairiku earthquake. In these figures, the thick and thin solid lines show the output models of the east-west and north-south components respectively, whereas the thin dotted lines show the input models of the east-west component. The input model was a simplified pulse from the surface seismometer reading, and the output model was a simplified wave obtained from the buried seismometer reading. For example, in Figure 6a, wave arrives at the ground surface and bottom of the well at 0 s and -0.253 s, respectively. Hence, the wave

propagation time from the bottom of the well to the surface is estimated as 0.253 s.

The propagation time during the Iwate-Miyagi Nairiku earthquake (Fig. 6c) was longer (0.346 s) than this initial propagation time. Figure 6b also shows a slight increase in the propagation time during the Sanriku-Minami earthquake. Peak ground accelerations at the Ichinoseki-Nishi site were more than 200 cm/s^2 during this event.

The peak of the output waveform in Figure 6e is not as clear as in the other results. We infer that incoherent scattering waves dominated over S waves propagating vertically during this time window and caused the unclear peak in the output waveform. This means that the amplitude of the peaks is a good indicator of the reliability of the estimated propagation times.

Note that no clear peaks can be seen in the positive time of all diagrams. These peaks are for the arrival of reflected waves generated at the ground surface and may be due to scattering and attenuation of seismic waves propagating between the two observation points. Hence, we focused only on the propagation times of the incidence waves.

Propagation times obtained from events before the Iwate-Miyagi Nairiku earthquake

Figure 7a shows the propagation times estimated by the NIOM analysis of the 279 events before the Iwate-Miyagi Nairiku earthquake. The horizontal axis is the order of occurrence. The solid circles and triangles in Figure 7b show the RMS values of the velocity amplitudes at the ground surface in the east-west and north-south directions, respectively, as a measure of the seismic intensity at each time window. Figure 7c shows the incidence angles of the direct S waves to the upper interface of the bedrock (i.e., the incidence angles to the bottom of the soil profile shown in Fig. 1). In this diagram, the open and solid circles indicate mantle earthquakes (depth $\geq$30 km) and crustal earthquakes (depth$<$30 km), respectively.

According to the S-wave velocity profile measured by well logging (Fig. 1), the propagation time of the S waves for a vertical incidence is 0.241 s, and this value is indicated by the dotted line in Figure 7a. Meanwhile, the propagation times obtained by the NIOM analysis are in the range of 0.25–0.265 s and is considerably larger than 0.241 s.

In Figure 6, we pointed out that the propagation times during the

Sanriku-Minami earthquake were about 0.27 s (0.274 s for the east-west component and 0.272 s for the north-south component), and we can confirm that these times are longer than the ordinary range of 0.25–0.265 s. This result can be attributed to the degradation of soil due to strong ground shaking of about 5 cm/s (RMS value of the velocity amplitudes in Fig. 7b). Moreover, the propagation times for the events right after it were in the ordinary range.

In contrast, the propagation times during the Miyagiken-Hokubu earthquake and its aftershocks, decreased to about 0.25 s (see Fig. 7a). As shown in Figure 7c, these earthquakes were crustal events, and the incidence angles at the Ichinoseki-Nishi site were about 60 degrees. Thus, the decrease in propagation time can be attributed to the oblique incidence of the seismic waves.

To examine the effect of the incidence angles, Figure 8 shows the relationship between the propagation times obtained by the NIOM analysis and the incidence angles of the direct S waves. Considering that the soil profile at the site consists of seven layers (Fig. 1), the following theoretical relationship can be derived from Snell's law:

$$
\begin{aligned}
T(\theta_8, \alpha) &= \sum_{i=7}^{1} \frac{H_i}{\alpha V_i} \cos\theta_i \\
&\sin\theta_i = \frac{V_i}{V_{i+1}} \sin\theta_{i+1}, \qquad V_8 = 3,200 \text{ (m/s)},
\end{aligned}
\tag{9}
$$

where V_i and θ_i are, respectively, the well-log S-wave velocities and the propagation angles with respect to the vertical axis in the i-th layer, T is the propagation time in the vertical array, α is the velocity correction factor for the well-log S-wave velocities. Subscript 8 in equation (9) indicates the properties of the bedrock layer added to the soil profile at the Ichinoseki-Nishi site, which corresponds to the surface layer in the regional ground structure model shown in Figure 3.

By putting α=1, equation (9) gives the theoretical propagation time for the soil profile measured by well logging. This result is shown as the dotted line in Figure 8. Comparison of this theoretical relationship with the observed results reveals that the theoretical propagation time is shorter than the observed ones by about 0.02 s; however, the relationships are similar in shape.

To compensate for the difference, we determined the velocity correction factor α by using the following fitting:

$$\sum_k \left\{T_{\mathrm{NIOM},k} - T(\theta_{8,k}, \alpha)\right\}^2 \rightarrow \min, \tag{10}$$

where $T_{\mathrm{NIOM},k}$ is the propagation time obtained by the NIOM analysis of the k-th event's records, and $\theta_{8,k}$ is the incidence angle at the k-th event. To avoid the nonlinear soil effect, the fitting calculation used only the events whose RMS values were smaller than

0.1 cm/s. As a result, the best-fitting α was 0.91, and the corresponding propagation time for a vertical incidence was 0.265 s. This result means that the S-wave velocities obtained by the NIOM analysis are smaller than the well-log S-wave velocities by about 10%. The solid lines in Figures 7a and 8 show respectively the propagation time and the best-fitting relationship $T(\theta, 0.91)$. The corresponding propagation time for vertical incidence can be calculated from the time for oblique incidence of angle θ by multiplying by a factor of $T(0, \alpha)/T(\theta, \alpha)$, in which α is 0.91. We refer to this as the 'vertical correction' and use it to eliminate the oblique incidence effect.

Temporal change in propagation time during the Iwate-Miyagi Nairiku earthquake

Figure 9 shows (a) the propagation times and (b) the RMS values of velocity amplitudes during the Iwate-Miyagi Nairiku earthquake, respectively. The horizontal axis is the time at the center of the time window.

Figure 9a shows a large increase in the propagation time. At 24 s, the propagation times peak and were 0.346 s for the east-west component and 0.342 s for the north-south component due to the nonlinear behavior of soil caused by the extremely strong shaking. The largest RMS values were 28.4 cm/s for the east-west component

and 27.7 cm/s for the north-south component in the time window from 20 s to 24 s. Soon after this time, the propagation time gradually decreased with decreasing seismic intensity. However, it should be noted that the propagation times in the coda part were still larger than the initial value of 0.265 s.

The propagation times for the coda part have a larger scatter than those before the Iwate-Miyagi Nariku earthquake as shown in Figure 7. Considering the relatively large RMS values during the coda part and that the Ichinoseki-Nishi site is situated above the fault plane, the large scatter can be attributed to both the soil degradation and the variation in the incidence angles associated with the rupture propagation.

Figure 10 shows the propagation times after the vertical corrections and the RMS values observed at the Ichinoseki-Nishi site during the Sanriku-Minami earthquake (M7.0, epicentral distance 74 km, depth 71 km). The incidence angle used in the vertical corrections was 34 degrees for all time intervals. During the principal motion, the propagation times increased to about 0.27 s due to strong ground motion (the largest RMS values were 5.0 cm/s for the east-west component and 4.0 cm/s for the north-south component); however, soon after the principal motion, the propagation times returned to the initial value. Considering that the largest RMS values during the Iwate-Miyagi

Nairiku earthquake were about 30 cm/s, the difference in the healing process after the nonlinear behavior of soil observed during the Iwate-Miyagi Nairiku earthquake and the Sanriku-Minami earthquake suggests that there is a critical strain level above which the nonlinear effects remain after the shaking stops.

Propagation times obtained from events after the Iwate-Miyagi Nairiku earthquake

Figure 11 shows (a) the propagation times before the vertical corrections, (b) the RMS values of the velocity amplitudes, and (c) the incidence angles of 179 events after the Iwate-Miyagi Nairiku earthquake in the same manner as in Figures 7 and 9. The horizontal axis is elapsed time in days after the earthquake. The time windows were 4 s.

Figure 11 shows a decreasing tendency in the uncorrected propagation times with elapsed time in spite of a large scatter in the propagation times. Similar to the results of the coda part of the mainshock, the large scatter in the propagation times can be attributed to the wider ranges of both the RMS values and the incidence angles because of the small hypocentral distances of the aftershocks. These effects have to be eliminated in order to ascertain the healing process of shear moduli of the soil.

Figure 12a shows the relationship between the propagation times before the

vertical correction and the incidence angles. The oblique incidence effect can clearly be seen in this diagram. Figure 12b shows the same relationship but with the propagation times after the vertical corrections were made. In this diagram, the dependency of the propagation time on the incidence angle was reduced. However, the decreasing tendency of the propagation times is still apparent, especially for the larger incidence angles. In Figure 8, there are much shorter propagation times than the theoretical for incidence angles more than about 60 degrees. These observations suggest that the vertical correction might not be enough for large incidence angles because of reflection and scattering at irregular interfaces near the ground surface. In addition, the propagation times still have a large scatter. Figure 12c shows the relationship between the corrected propagation times and the RMS values of the velocity amplitudes. In this diagram, no dependency of the propagation times on the RMS values less than 0.1 cm/s is seen; however, an increasing tendency of the propagation times with increasing RMS values for the RMS values more than 0.1 cm/s can be seen. This result suggests that the soil degradation at this site is caused by ground motion with velocity amplitudes more than 0.1 cm/s. Considering that the value is an important property regarding the nonlinear behavior of soils, an analysis of different vertical array records should be conducted. Figure 12d shows the propagation

times after the correction as a function of incidence angle for the RMS values lower than 0.1 cm/s. The decreasing tendency of the propagation times with increasing incident angle that is seen in Figure 12 is no longer apparent.

Figure 13a shows the propagation times for the events before the 2008 Iwate-Miyagi Nairiku earthquake. It is similar to what is shown in Figure 7a, but with vertical corrections. The propagation times are distributed around the initial value of 0.265 s with a lesser scatter than that shown in Figure 7a. Figure 13b shows the relationship between elapsed time after the mainshock and corrected propagation times whose RMS values are smaller than 0.1 cm/s. In this diagram, the results for incidence angles larger than 60 degrees were removed to avoid the effects of incidence angles that could not be corrected as in Figure 12b. A relatively large scatter remains possibly because there were irregular interfaces near the surface and small errors in estimating the hypocenter locations cause the actual and estimated incidence angles to be different for near and shallow aftershocks.

This diagram does not show the clear decreasing tendency of propagation time with elapsed time that is apparent in Figure 11a, and the propagation time remains longer than the initial value of 0.265 s by about 0.015 s. This result means that the decreasing

tendency of the propagation time in Figure 11a can be attributed to a decrease in the intensity of strong ground motion associated with the temporal decay of the aftershock activities, and the shear rigidities of soils remained lower than their initial values before the earthquake for more than a year.

Relationship between shear modulus and shear strain

The relationship between shear modulus and shear strain was examined on the basis of the propagation times obtained by the NIOM analysis. Because the seismometers are installed only at the surface and at the bottom of the deep well at the KiK-net Ichinoseki-Nishi site, it is impossible to evaluate the degradations at each layer separately from the propagation times. As shown in Figure 1, the S-wave velocities from the surface to the 64-m depth ranged from 430 m/s to 680 m/s (we call these layers, 'upper soil layers'), and the impedance contrast with the underlying bedrock layers is clear (we call these layers, 'bedrock layers'). Therefore, we assumed that the degradations of shear moduli occurred evenly and only in the upper soil layers.

The analysis of the events before the Iwate-Miyagi Nairiku earthquake revealed that the propagation time through the vertical array was 0.265 s, and the value of α was

0.91. Accordingly, the vertical propagation times in the upper soil layers, T_s, and the bedrock layers, T_b, are 0.122 s and 0.143 s, respectively. By using T_s and T_b, the actual S-wave velocity in the upper soil layers, v, can be written as

$$v = V\alpha\beta, \qquad \beta = \frac{T_s}{T_{\text{NIOM}} - T_b}, \tag{11}$$

where T_{NIOM} is the propagation time obtained by the NIOM analysis, and V is the S-wave velocity measured by well logging. For example, the actual S-wave velocity in the second layer (530 m/s by the well logging) is 530α=482 m/s before the Iwate-Miyagi Nairiku earthquake. The propagation time T_{NIOM} during the mainshock reached about 0.35 s (22 s for the east-west component, as shown in Fig. 9a); this corresponds to

$$\beta = \frac{0.122}{0.35 - 0.143} = 0.59 \tag{12}$$

and an S-wave velocity of 530$\alpha\beta$=482β=284 m/s.

Using the S-wave velocity v obtained by the above procedure, the normalized shear modulus can be written as

$$G/G_0 = v^2/(V\alpha)^2 = \beta^2, \tag{13}$$

where $V\alpha$ is the S-wave velocity at an infinitesimal strain level.

Because shear strain is not observed at the site, we defined average strain $\overline{\varepsilon}$ as

$$\overline{\varepsilon} = v_{\mathrm{RMS}}/v, \tag{14}$$

where v_{RMS} is the RMS value of the velocity waveform during the corresponding time window. Equation (14) is based on the one-dimensional propagation of seismic waves, as determined by

$$\varepsilon = \frac{\partial u(z,t)}{\partial z} = \frac{\partial u(z,t)}{\beta\, \partial t}, \tag{15}$$

where u is the displacement of seismic waves and z is the coordinate axis along the wave propagation direction.

Figure 14 shows the relationships between the shear strain and the normalized shear modulus for the second layer obtained from the propagation times (a) for events before, (b) during, and (c) for the events after the mainshock of the Iwate-Miyagi Nairiku earthquake. For the events before and after the mainshock, the propagation times with vertical corrections were used to evaluate the shear strains and shear moduli.

Before the mainshock, most of the shear strain values are below 1×10^{-5}, and no soil degradation is apparent at this strain level (e.g., Ishihara, 1996). During the mainshock, the shear strain reached about 1×10^{-3} soon after the arrival of the S-wave, and the shear modulus decreased to 40% of the initial value. The shear modulus then

gradually increased to around 70% to 80% of the initial value as shear strain decreased to 1×10^{-5} according to the decay of the ground motions. After the mainshock, the shear modulus eventually settled to around 80% of the initial value.

It should be noted that the NIOM results for the events before the Iwate-Miyagi Nairiku earthquake revealed that the S-wave velocities are 10% lower than those provided by the well-log (see Figure 8), and this difference was distributed evenly with respect to the S-wave velocities over the entire soil column. To examine the effect of this hypothesis, we assumed that the observed difference in the propagation time was caused by errors in the S-wave velocities only of the upper soil layers and calculated the corresponding S-wave velocities. By setting α in equation 9 for the bedrock layers to unity, the fitting calculation (equation 10) yielded an α for the upper soil layers of 0.83. Therefore, under this hypothesis, the S-wave velocities in the upper soil layers are smaller than those obtained by the well-log by 17%, and T_s and T_b in equation 11 are 0.134 s and 0.132 s, respectively. For the propagation time T_{NIOM} of 0.35 s, β for the above results is estimated as

$$\beta = \frac{0.134}{0.35 - 0.132} = 0.61, \tag{16}$$

whereas the value of β in equation 12 is 0.59. Because the normalized shear modulus

is given by β^2, the hypothesis placed on the initial S-wave velocities does not cause a significant difference in the estimation of the normalized shear modulus. The estimation of the shear strains using equation 14 will also be affected by the S-wave velocities; however, the difference between the estimated strains is negligible on the logarithmic scale used in Figure 14.

Nonlinear soil behavior at a large strain level has been examined by researchers mainly in laboratory tests (e.g., Seed and Idriss, 1970; Sun et al., 1988; Hardin and Drnevich, 1972a, 1972b; and Ishihara, 1996). We compared our results with those of laboratory tests conducted by Hatanaka et al. (1988) on soil with similar properties to those at the Ichinoseki-Nishi site. The test specimens in their research were taken from a diluvial gravel deposit called Tokyo gravel by using the in-situ freezing method. The depth of the deposit was 18.5 m from the ground surface, and the in-situ S-wave velocity and wet unit weight were reported as 380 m/s and 2.26×10^3 kg/m^3, respectively. Both undisturbed specimens and reconstituted specimens having the same relative density of about 55% were used in their undrained cyclic tests using a triaxial test apparatus.

Figure 14d shows their results on the relationship between the shear modulus and shear strain. In their laboratory tests, the shear modulus decreased by 65% for a

confining stress of 5 kgf/cm^2 and by 50% for a stress of 3 kgf/cm^2 at a strain of 1×10^{-3}. In our results, the shear modulus fell by about 60% of the initial value at the same strain level, and hence, it is consistent with the nonlinear soil behavior revealed by their laboratory tests.

Comparing the results for the undisturbed and reconstituted specimens in Figure 14d, we see that the undisturbed specimen has a shear modulus that is 30% larger than the reconstituted one. This means that disturbances reduce the shear modulus at an infinitesimal strain by affecting the soil structure. The shear modulus reduction of 20% in going from the events before and after the Iwate-Miyagi Nariku earthquake can be attributed to the disturbance effect.

Conclusion

We examined temporal changes in the propagation times of S waves on the basis of vertical array records observed at the KiK-net Ichinoseki-Nishi site during 459 events from 21 July 2000 to 19 October 2009, including the 14 June 2008 Iwate-Miyagi Nairiku earthquake. The major conclusions of this study are as follows:

1) The NIOM analysis of the events before the Iwate-Miyagi Nairiku earthquake revealed that the propagation time of S waves for vertical incidence was 0.265 s, and the corresponding S-wave velocities are smaller than the well-log S-wave velocities by about 10%.

2) During the principal motion of the Iwate-Miyagi Nairiku earthquake, the propagation times abruptly increased to 0.346 s for the east-west component and 0.342 s for the north-south component. This result can be attributed to the nonlinear soil behavior caused by the extremely strong shaking. Additionally, a gradual decrease in propagation time with a decreasing seismic intensity was observed soon after the principal motions. However, the propagation times in the coda part were still larger than the initial value.

3) A slight increase in propagation time was also observed during the principal motion of the Sanriku-Minami earthquake; however, the propagation time returned to the initial value soon after the principal motion. The difference in the nonlinear soil behavior observed during the Iwate-Miyagi Nairiku earthquake and the Sanriku-Minami earthquake suggests that there is a critical strain level above which nonlinear effects remain after the shaking stops.

4) The results obtained by the NIOM analysis for the events after the Iwate-Miyagi Nairiku earthquake showed that propagation times were longer than the initial value but that it tended to decrease with elapsed time.

5) In spite of 4), the corrected propagation times for S waves whose RMS values were smaller than 0.1 cm/s did not show a decreasing tendency with elapsed time. Thus, we concluded that the decrease in propagation times with elapsed time was due to the decrease in the intensity of strong ground motions associated with the temporal decay of aftershock activities, and the shear rigidities of the soil remained less than in the initial state for more than a year.

6) The shear strain and shear modulus of the upper soil layers were estimated from the propagation times. The results revealed that the shear strain reached about 1×10^{-3} soon after the S-wave arrived, and the shear modulus decreased to 40% of the initial value during the principal motion of the Iwate-Miyagi Nairiku earthquake. The shear modulus then gradually increased to around 70% to 80% of the initial value as the ground motion decayed. After that, the shear modulus remained around 80% of the initial value for more than a year.

7) A comparison with laboratory tests conducted by Hatanaka et al. (1988) led us

to conclude that the aforementioned 20% reduction of shear moduli after the Iwate-Miyagi Nairiku earthquake can be attributed to the disturbance caused by extremely strong ground shaking during the earthquake.

Data and Resources

The accelerograms analyzed in this study and further information on the observation system can be found at the web site http://www.kik.bosai.go.jp/kik/index_en.html (last accessed July 2012).

Acknowledgments

The authors would like to thank the National Research Institute for Earth Science and Disaster Prevention (NIED) for providing the accelerograms used in this study. The authors would also like to thank Dr. Arthur McGarr and two anonymous reviewers for their helpful suggestions on improving the manuscript.

REFERENCES

Aki, K. and P. G. Richards (1980). *Quantitative Seismology: Theory and Methods*, 1, W. H. Freeman, New York.

Aoi, S., T. Kunugi, and H. Fujiwara (2008). Trampoline effect in extreme ground motion, *Science* **322**, 727–730.

Bouchon, M. and K. Aki (1977). Discrete wave-number representation of seismic-source wave fields, *Bull. Seism. Soc. Am.* **67**, 259–277.

Haddadi, H. R. and H. Kawakami (1998a). Modeling wave propagation by using Normalized Input-Output Minimization (NIOM) method for multiple linear systems, *Structural Eng./Earthquake Eng.* **15**, no 1, 29s–39s.

Hadaddi, H. R. and H. Kawakami (1998b). Effect of liquefaction on ground motion during the Hyogoken-nanbu earthquake, 1995, in Japan by using the NIOM method, The Effect of Surface Geology on Seismic Motion, Irikura, Kudo, Okada and Sasatani (editors), Balkema, Rotterdam, **2**, 1015–1022.

Hardin, B. O. and V. P. Drnevich (1972a). Shear modulus and damping in soils: measurement and parameter effects, *J. Soil Mech. Foundations Div.* **98**, 603–624.

Hardin, B. O. and V. P. Drnevich (1972b). Shear modulus and damping in soils: design

equations and curves, *J. Soil Mech. Foundations Div.* **98**, 667–692.

Hasegawa, A., N. Umino, and A. Takagi (1978). Double-planed structure of the deep seismic zone in the northeastern Japan Arc, *Tectonophysics* **47**, 43–58.

Haskell, N. A. (1953). The dispersion of surface waves on multilayered media, *Bull. Seism. Soc. Am.* **43**, 17–34.

Hatanaka, M., Y. Suzuki, T. Kawasaki, and M. Endo (1988). Cyclic undrained shear properties of high quality undisturbed Tokyo gravel, *Soils and Foundations* **28**, 4, 57–68.

Ishihara, K. (1996). *Soil behaviour in earthquake geotechnics*, Oxford University Press, New York.

Katayama, I., F. Fukui, M. Satoh, Y. Makihara, and K. Tokimatsu (1986). Comparison of dynamic soil properties between undisturbed and disturbed dense sand samples, *Proc. 21st Annual Conf. of JSSMFE*, 583–584 (*in Japanese*).

Kawakami, H. and P. Bidon (1997). A simplified input output relation method using AR model for earthquake wave propagation analysis, *Earthq. Engng. Struct. Dyn.* **26**, 1041–1057.

Kawakami, H. and H. R. Haddadi (1998). Modeling wave propagation by using

normalized input-output minimization (NIOM), *Soil Dyn. Earthq. Engng.* **17**, 117–126.

KiK-net (2000). http://www.kik.bosai.go.jp/kik/index_en.html (last accessed July 2012).

Langston, C. A. (1979). Structure under Mount Rainier, Washington, inferred from teleseismic body waves, *J. Geophys. Res.* **84**, 4749–4762.

Mogi, H., S. M. Shrestha, H. Kawakami, and S. Okamura (2010). Nonlinear soil behavior observed at vertical array in the Kashiwazaki-Kariwa Nuclear Power Plant during the 2007 Niigata-ken Chuetsu-oki earthquake, *Bull. Seism. Soc. Am.* **100**, 762–775.

NIED (National Research Institute for Earth Science and Disaster Prevention) (2008). Topics–Past Large Earthquakes, http://www.kyoshin.bosai.go.jp/cgi-bin/kyoshin/bigeqs/index.cgi?E (last accessed July 2012)

Ohmachi, T., S. Inoue, K. Mizuno, and M. Yamada (2011). Estimated cause of extreme acceleration records at the KiK-net IWTH25 station during the 2008 Iwate-Miyagi Nairiku earthquake, Japan, *J. JAEE* **11**, 32–47 (*in Japanese*).

Pavlenko, O. V. and K. Irikura (2002). Changes in shear moduli of liquefied and nonliquefied soils during the 1995 Kobe earthquake and its aftershocks at three

vertical-array sites. *Bull. Seism. Soc. Am.* **92**, 1952–1969.

Pavlenko, O. V. and K. Irikura (2006). Nonlinear behavior of soils revealed from the records of the 2000 Tottori, Japan, earthquake at stations of the digital strong-motion network KiK-net, *Bull. Seism. Soc. Am.* **96**, 2131–2145.

Satoh, T., M. Fushimi, and Y. Tatsumi (2001). Inversion of strain-dependent nonlinear characteristics of soils using weak and strong motions observed by borehole sites in Japan, *Bull. Seism. Soc. Am.* **91**, 365–380.

Satoh, T. (2006). Inversion of Qs of deep sediments from surface-to-borehole spectral ratios considering obliquely incident SH and SV waves, *Bull. Seism. Soc. Am.* **96**, 943–956.

Seed, H. B. and I. M. Idriss (1970). Soil moduli and damping factors for dynamic response analyses, Report no. EERC 70-10, Earthquake Engineering Research Center, University of California, Berkeley, California.

Sun, J. I., R. Golesorkhi, and H. B. Seed (1988). Dynamic moduli and damping ratios for cohesive soils, Report no. EERC 88-15, Earthquake Engineering Research Center, University of California, Berkeley, California.

Suzuki, W., S. Aoi, and H. Sekiguchi (2010). Rupture process of the 2008 Iwate-Miyagi

Nairiku, Japan, earthquake derived from near-source strong-motion records, *Bull. Seism. Soc. Am.* **100**, 256–266.

Tokimatsu, K., H. Arai, and K. Minowa (2008). Soil nonlinearity and bedrock strong motions estimated from downhole array records at Kashiwazaki-Kariwa nuclear power plant during the 2007 Niigata-ken Chuetsu-oki earthquake, *J. Struct. Constr. Eng.* **73**, 1273–1280 (*in Japanese*).

Tokimatsu, K. and H. Arai (2008). Nonlinear soil properties estimated from downhole array recordings at Kashiwazaki-Kariwa nuclear power plant in the Niigaka-ken Chuetsu-oki arthquakes, *Proc. 14th WCEE*, Beijing, China, http://www.nicee.org/wcee/2008 (last accessed July 2012).

Yamada, S., J. Mori, and T. Heaton (2009). The slapdown phase in high-acceleration records of large earthquakes, *Seism. Res. Lett.* **80**, 559–563.

Author affiliations:

Hidenori Mogi

Department of Civil and Environmental Engineering, Saitama University

255 Shimo-ohkubo Sakura-ku Saitama-shi Saitama 338-8570, Japan

hmogi-2008f@kiban.civil.saitama-u.ac.jp

Santa Man Shrestha

Department of Civil Engineering, Acme Engineering College

Kathmandu, Nepal.

Hideji Kawakami

Geosphere Research Institute, Saitama University

255 Shimo-ohkubo Sakura-ku Saitama-shi Saitama 338-8570, Japan

Jun'ya Kawamura

Saitama City Government,

6-4-4 Tokiwa Urawa-ku Saitama-shi Saitama 330-9588, Japan

List of Figures

function. The results for the far and shallow source (L=200 km and D=20 km) also show the waveforms due to the refracted waves and reflected waves.

Figure 4 Epicenters of analyzed events before the 14 June 2008 Iwate-Miyagi Nairiku earthquake. The total number of events is 279. Two major earthquakes—the 26 May 2003 Sanriku-Minami earthquake (M7.0, depth 71 km) and the 26 July 2003 Miyagiken-Hokubu earthquake (M6.2, depth 12 km)—are included.

Figure 5 Epicenters of the 2008 Iwate-Miyagi Nairiku earthquake and events after it. The fault plane shown in the diagram was proposed by Suzuki et al. (2010). Most of the events are aftershocks of the Iwate-Miyagi Nairiku earthquake. The total number of analyzed events is 180.

Figure 6 Simplified input and output waveforms estimated by the NIOM analysis for (a) the events on July 21, 2000, 3:39 (M=6.0, L=277 km, D=49 km), (b) the 2003 Sanriku-Minami earthquake (May 26, 18:24, M=7.0, L=74 km, D=71 km), (c-f) the principal motion (20–24 s) and coda parts (84–88 s, 186–190 s, and 278–282 s) of the 2008 Iwate-Miyagi Nairiku earthquake, (g) the aftershock of the

2008 Iwate-Miyagi Nairiku earthquake on June 14, 2008, 9:30 (M=4.0, L=16 km, D=7 km), and (h) the event on June 1, 2009, 0:33 (M=4.6, L=152 km, D=59 km). In these diagrams, the thick solid line and thin solid line show the output model for the east-west and north-south components, respectively, and the thin dotted line shows the input model of the east-west component. The peak value A_{NIOM} and the corresponding time T_{NIOM} in the output model of the east-west component are also shown in each diagram.

Figure 7 (a) Propagation times estimated by NIOM analysis of the S-wave parts in the accelerograms of events before the 2008 Iwate-Miyagi Nairiku earthquake. (b) RMS values of the velocity amplitudes at each time window. (c) Incidence angles of direct S waves theoretically estimated by using a horizontally layered ground structure. In diagrams (a) and (b), the circles and triangles show the results for the east-west and north-south components, respectively. The solid symbols mean that the peak values of the NIOM output waveform, A_{NIOM}, are larger than 0.1, whereas the open symbols mean the values are less than 0.1. In diagram (c), the open circles and solid circles indicate mantle earthquakes (depth $\geq$ 30 km) and crustal earthquakes (depth $<$ 30 km).

Figure 8　Relationship between the propagation time estimated by NIOM analysis (shown in Fig. 7a) and incidence angle of the direct S wave (shown in Fig. 7c). The dotted and solid lines show the theoretical relationship based on the S-wave velocities measured by well logging and those obtained by fitting, respectively.

Figure 9　(a) Propagation times during the 2008 Iwate-Miyagi Nairiku earthquake estimated by NIOM analysis. (b) RMS values of velocity amplitudes during each time window.

Figure 10 (a) Propagation times (after the vertical corrections for an incidence angle of 34 degrees) obtained from the records observed at the Ichinoseki-Nishi site during the 2003 Sanriku-Minami earthquake. (b) RMS values of velocity amplitudes during each time window.

Figure 11 (a) Propagation times (before the vertical corrections) obtained from the events after the 2008 Iwate-Miyagi Nairiku earthquake. (b) RMS values of the velocity amplitudes during each time window. (c) Incidence angles of direct S waves theoretically estimated by using a horizontally layered ground structure.

Figure 12 (a) Relationship between incidence angles and uncorrected propagation

times observed during the events after the Iwate-Miyagi Nairiku earthquake. (b) Similar relationship to the one shown in diagram (a) but with vertical corrections to the propagation times. (c) Relationship between corrected propagation times and RMS values of the velocity amplitudes. (d) Relationship between corrected propagation times and incidence angles whose RMS values are lower than 0.1 cm/s.

Figure 13 (a) Propagation times of the events before the 2008 Iwate-Miyagi Nairiku earthquake. These are similar to what is shown in Figure 7a but have vertical corrections. (b) Relationship between elapsed days and propagation times. This diagram is analogous to Figure 11a, but includes only results whose RMS values and incidence angles were less than 0.1 cm/s and 60 degrees, respectively.

Figure 14 Relationship between shear strains and normalized shear moduli in the second layer obtained from (a) events before, (b) during, and (c) after the mainshock of the 2008 Iwate-Miyagi Nairiku earthquake. For the events before and after the mainshock, the propagation times after vertical corrections were used to evaluate the shear strains and shear moduli. (d) Relationship between shear strains and shear moduli obtained in laboratory tests of undisturbed and

reconstituted specimens of Tokyo gravel by Hatanaka et al. (1988) [Reprinted from *Soils and Foundations*, **28**, 4, p. 67, Fig. 13, courtesy of Prof. Hatanaka].

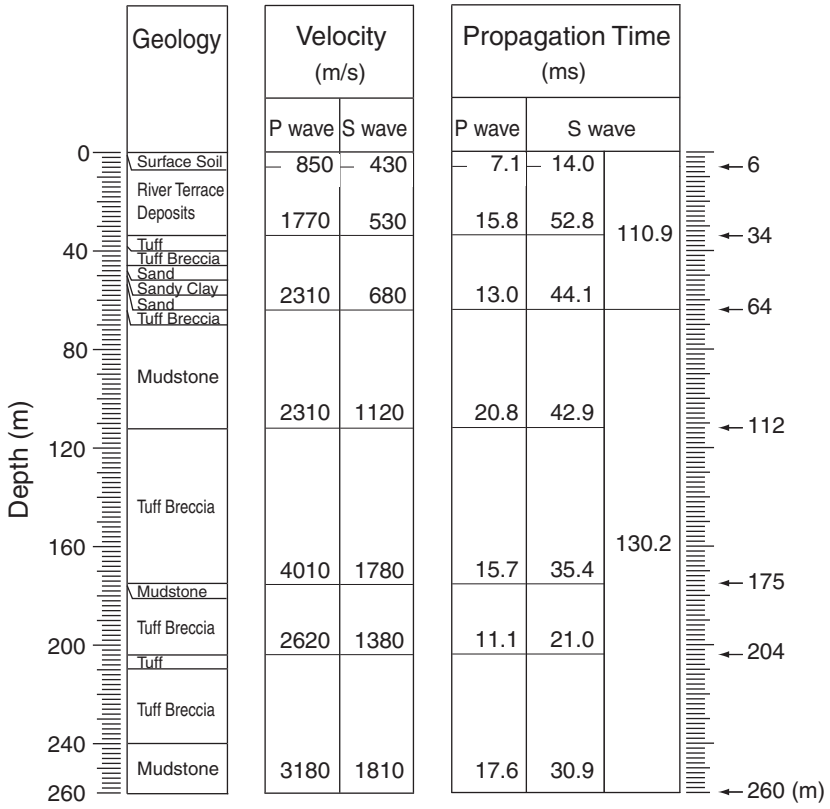

Figure 1. Soil profile at the KiK-net Ichinoseki-Nishi vertical array (KiK-net, 2000). The propagation time was added by the authors.

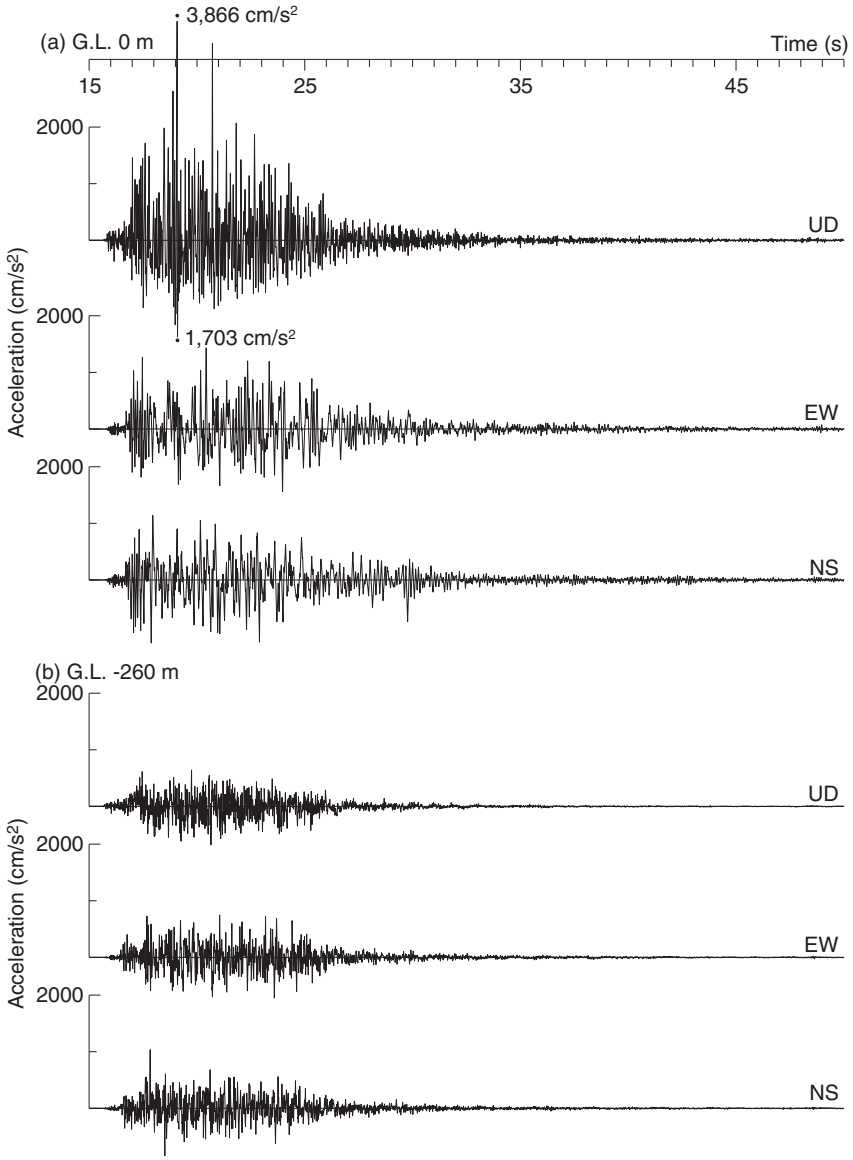

Figure 2. Principal parts of the accelerograms of the 2008 Iwate-Miyagi Nairiku earthquake observed at the Ichinoseki-Nishi vertical array. Diagrams (a) and (b) show the accelerograms at the ground surface and at the bottom of the well (GL-260 m), respectively. The peak ground accelerations at the ground surface in up-down, east-west, and north-south directions were respectively 3,866 cm/s^2, 1,432 cm/s^2, and 1,143 cm/s^2, and those at the bottom were 681 cm/s^2, 748 cm/s^2, and 1,036 cm/s^2, respectively. The waveform of the up-down component observed at the ground surface shows asymmetric peak accelerations of 3,866 cm/s^2 in the upward direction and 1,703 cm/s^2 in downward direction.

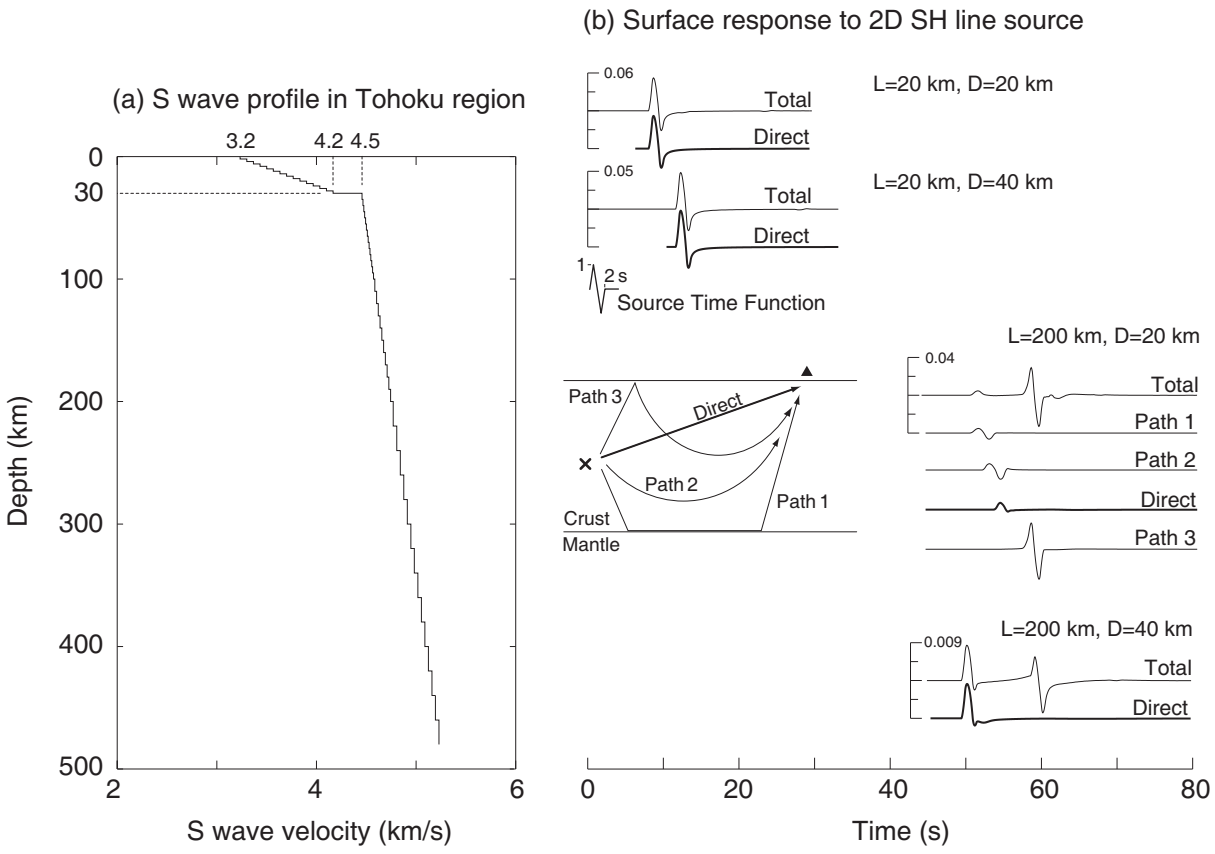

Figure 3. (a) Velocity profile in the Tohoku region used to calculate incidence angles. (b) Examples of the calculated waveforms of the total waves (thin lines) and the direct S phase (thick lines) for SH line sources with a double triangular time function. The results for the far and shallow source (L=200 km and D=20 km) also show the waveforms due to the refracted waves and reflected waves.

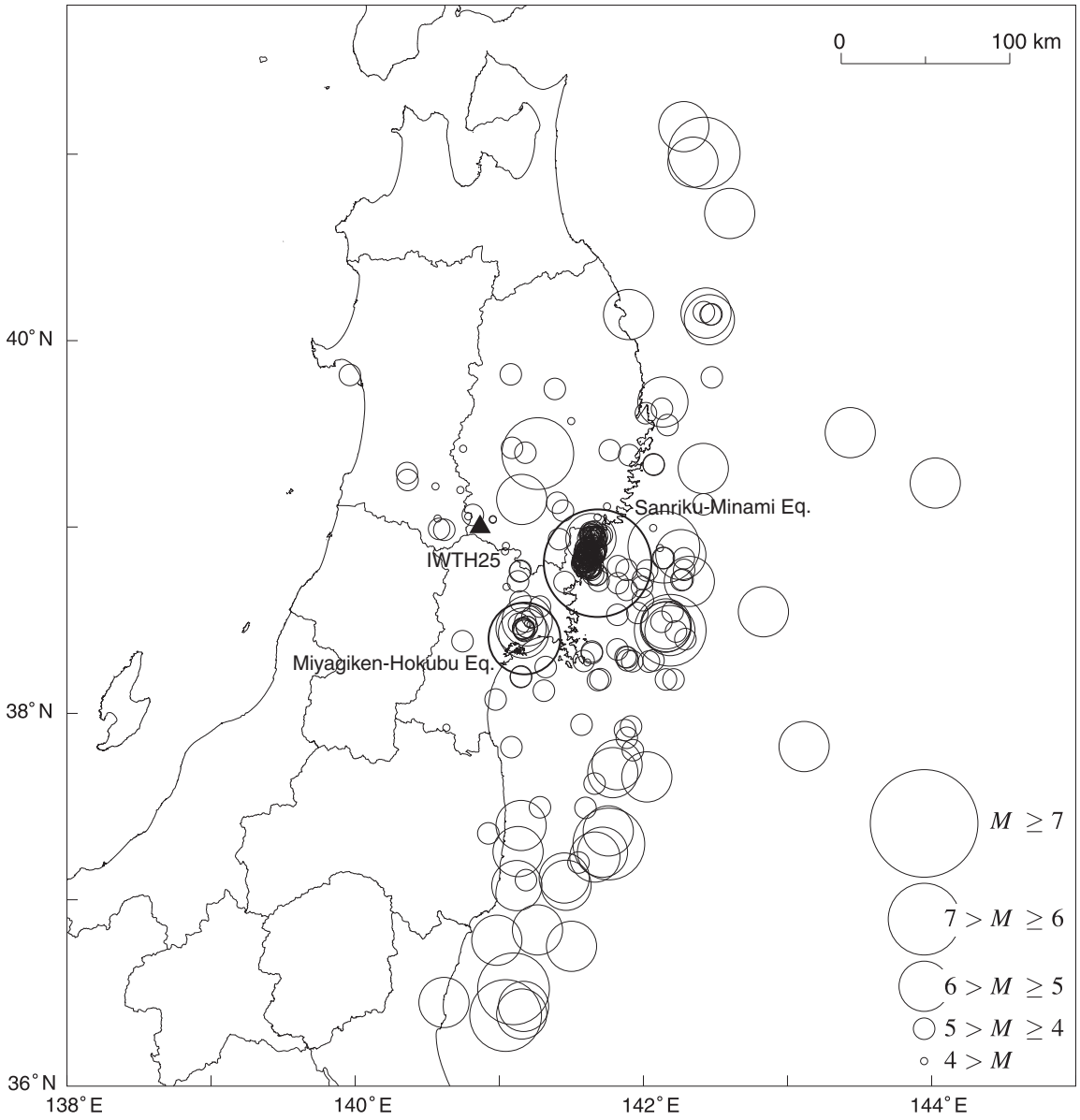

Figure 4. Epicenters of analyzed events before the 14 June 2008 Iwate-Miyagi Nairiku earthquake. The total number of events is 279. Two major earthquakes—the 26 May 2003 Sanriku-Minami earthquake (M7.0, depth 71 km) and the 26 July 2003 Miyagiken-Hokubu earthquake (M6.2, depth 12 km)—are included.

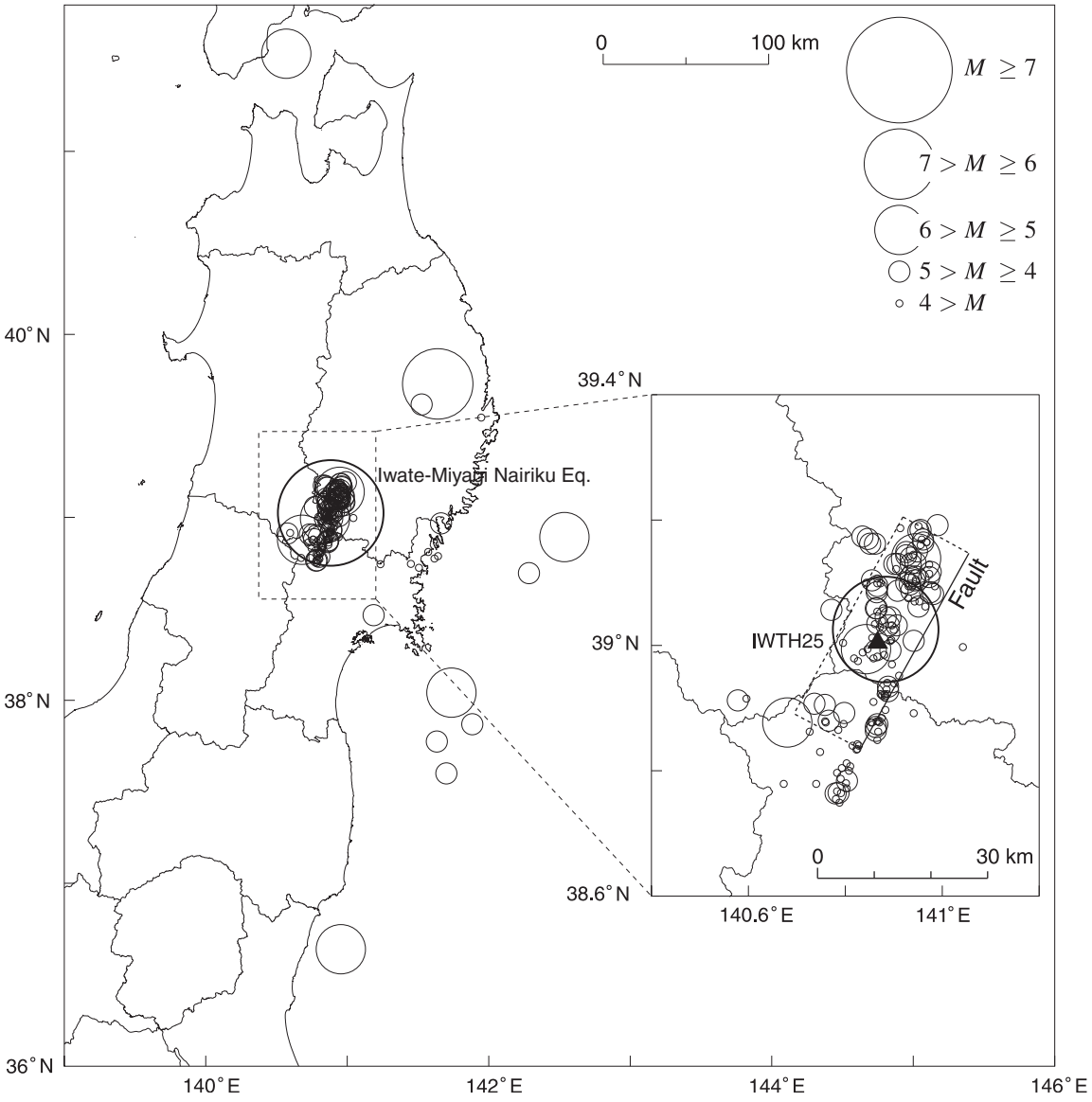

Figure 5. Epicenters of the 2008 Iwate-Miyagi Nairiku earthquake and events after it. The fault plane shown in the diagram was proposed by Suzuki et al. (2010). Most of the events are aftershocks of the Iwate-Miyagi Nairiku earthquake. The total number of analyzed events is 180.

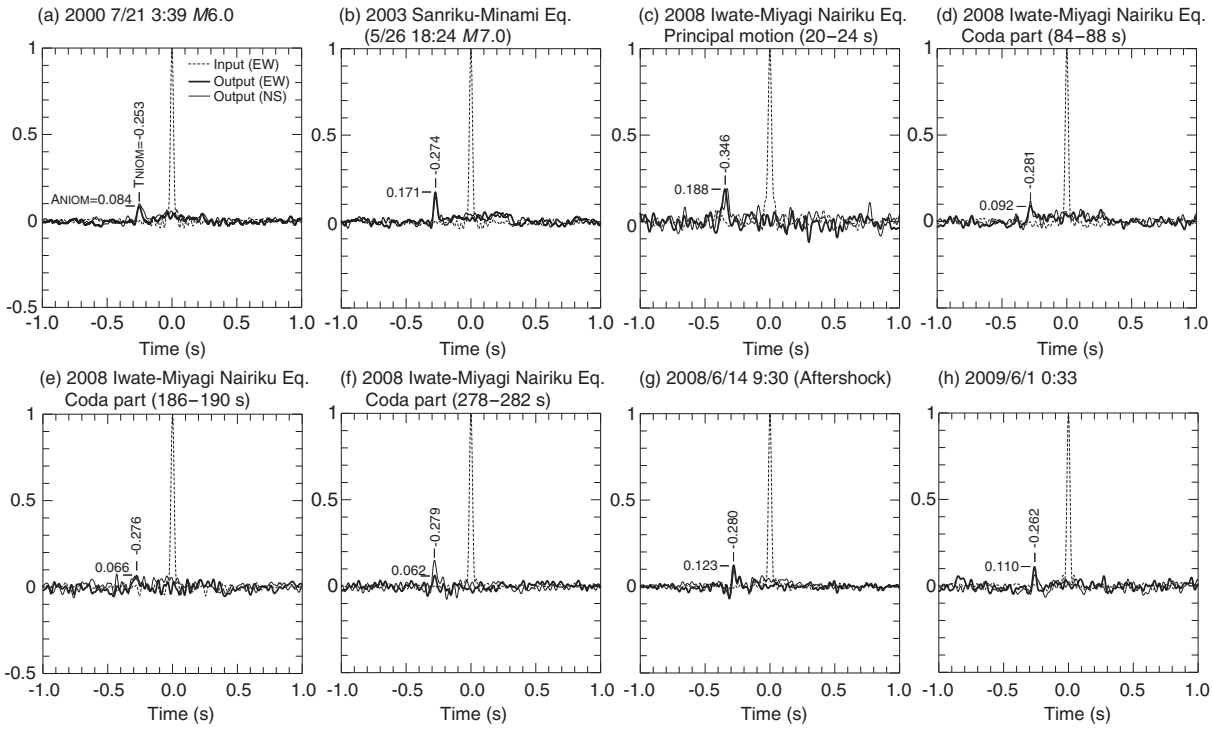

Figure 6. Simplified input and output waveforms estimated by the NIOM analysis for (a) the events on July 21, 2000, 3:39 (M=6.0, L=277 km, D=49 km), (b) the 2003 Sanriku-Minami earthquake (May 26, 18:24, M=7.0, L=74 km, D=71 km), (c-f) the principal motion (20–24 s) and coda parts (84–88 s, 186–190 s, and 278–282 s) of the 2008 Iwate-Miyagi Nairiku earthquake, (g) the aftershock of the 2008 Iwate-Miyagi Nairiku earthquake on June 14, 2008, 9:30 (M=4.0, L=16 km, D=7 km), and (h) the event on June 1, 2009, 0:33 (M=4.6, L=152 km, D=59 km). In these diagrams, the thick solid line and thin solid line show the output model for the east-west and north-south components, respectively, and the thin dotted line shows the input model of the east-west component. The peak value A_{NIOM} and the corresponding time T_{NIOM} in the output model of the east-west component are also shown in each diagram.

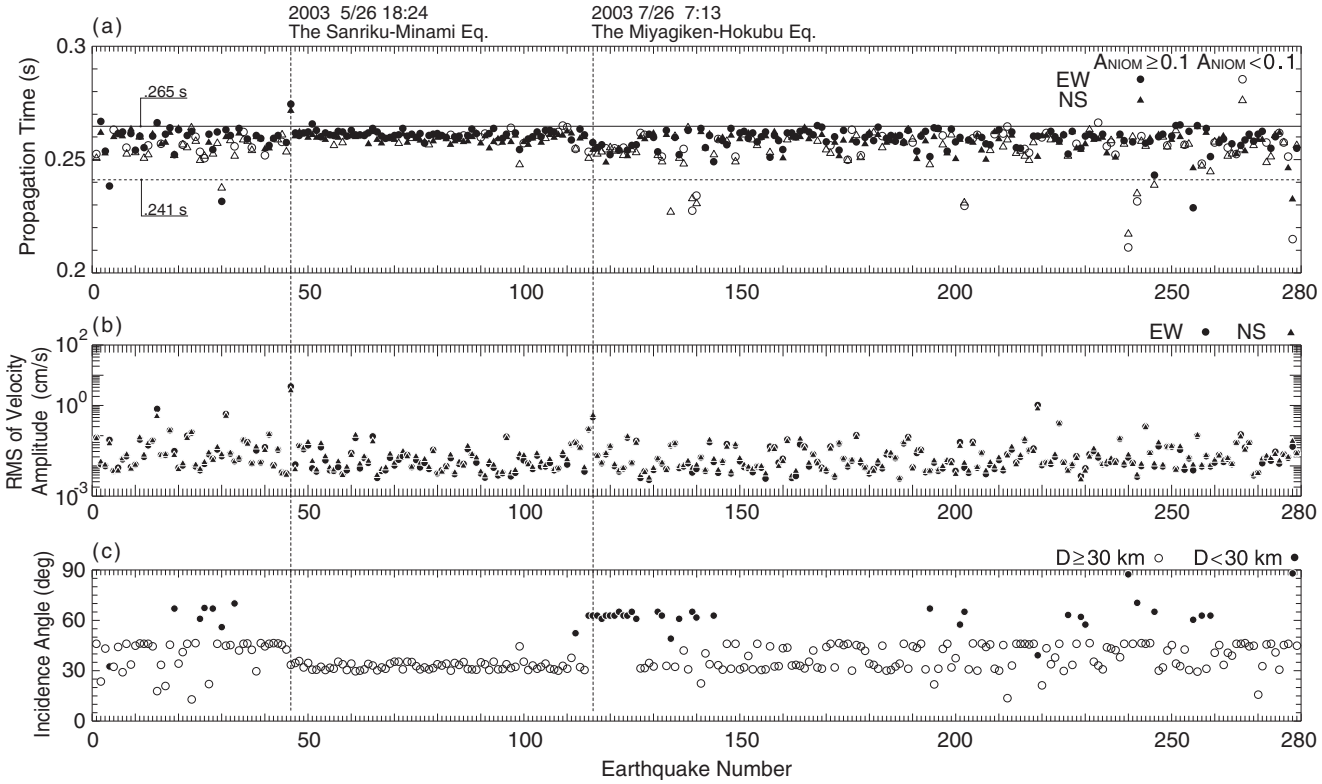

Figure 7. (a) Propagation times estimated by NIOM analysis of the S-wave parts in the accelerograms of events before the 2008 Iwate-Miyagi Nairiku earthquake. (b) RMS values of the velocity amplitudes at each time window. (c) Incidence angles of direct S waves theoretically estimated by using a horizontally layered ground structure. In diagrams (a) and (b), the circles and triangles show the results for the east-west and north-south components, respectively. The solid symbols mean that the peak values of the NIOM output waveform, A_{NIOM}, are larger than 0.1, whereas the open symbols mean the values are less than 0.1. In diagram (c), the open circles and solid circles indicate mantle earthquakes (depth $\geq$ 30 km) and crustal earthquakes (depth $<$ 30 km).

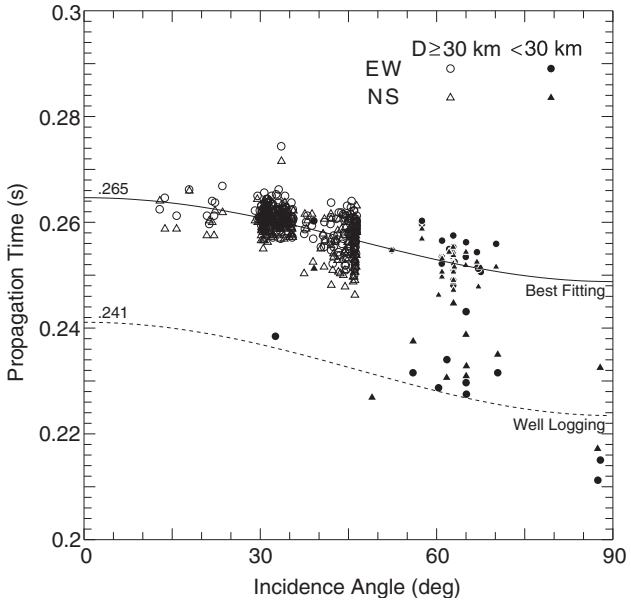

Figure 8. Relationship between the propagation time estimated by NIOM analysis (shown in Fig. 7a) and incidence angle of the direct S wave (shown in Fig. 7c). The dotted and solid lines show the theoretical relationship based on the S-wave velocities measured by well logging and those obtained by fitting, respectively.

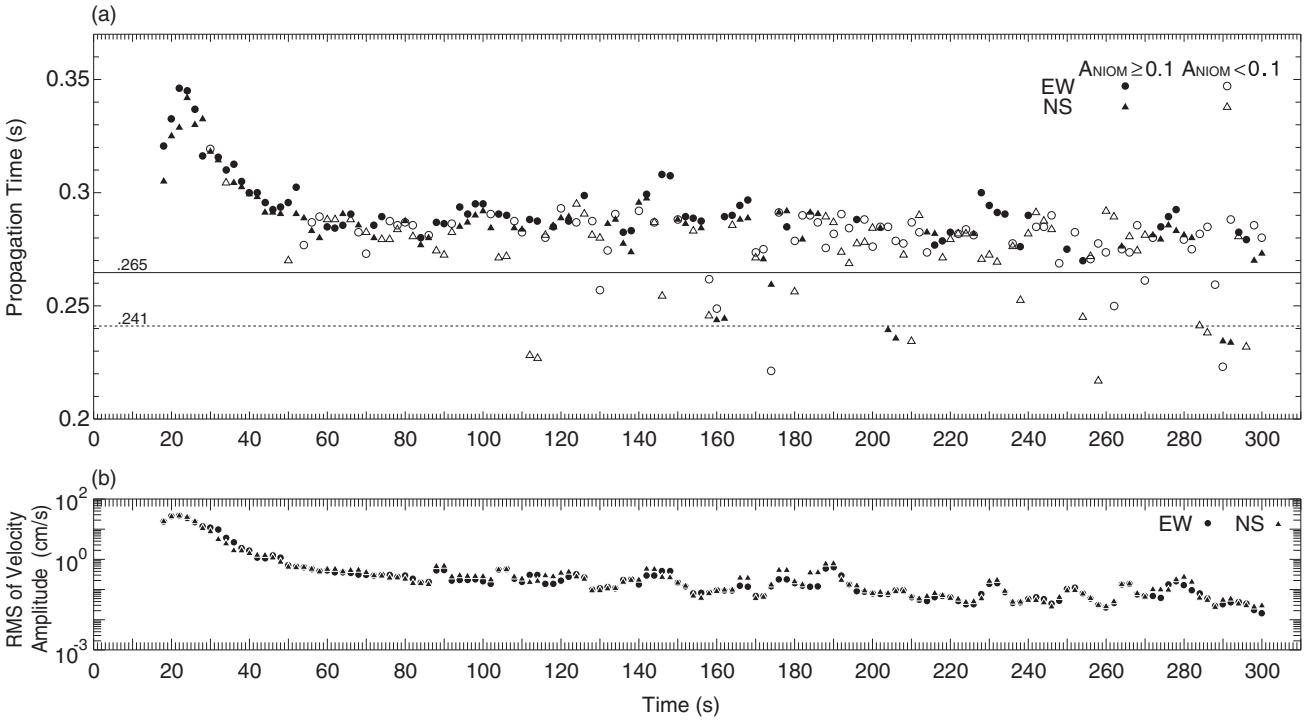

Figure 9. (a) Propagation times during the 2008 Iwate-Miyagi Nairiku earthquake estimated by NIOM analysis. (b) RMS values of velocity amplitudes during each time window.

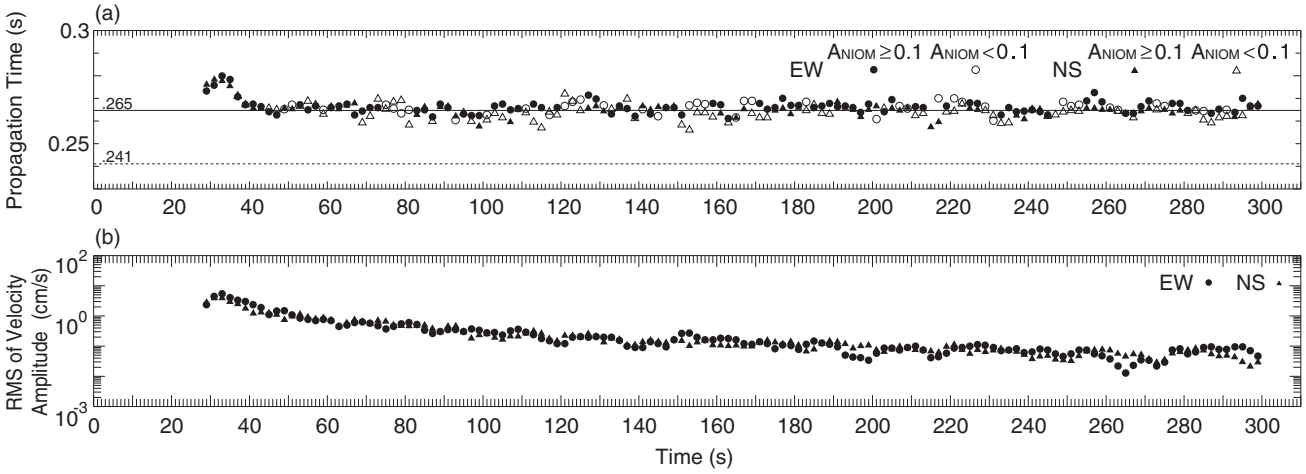

Figure 10. (a) Propagation times (after the vertical corrections for an incidence angle of 34 degrees) obtained from the records observed at the Ichinoseki-Nishi site during the 2003 Sanriku-Minami earthquake. (b) RMS values of velocity amplitudes during each time window.

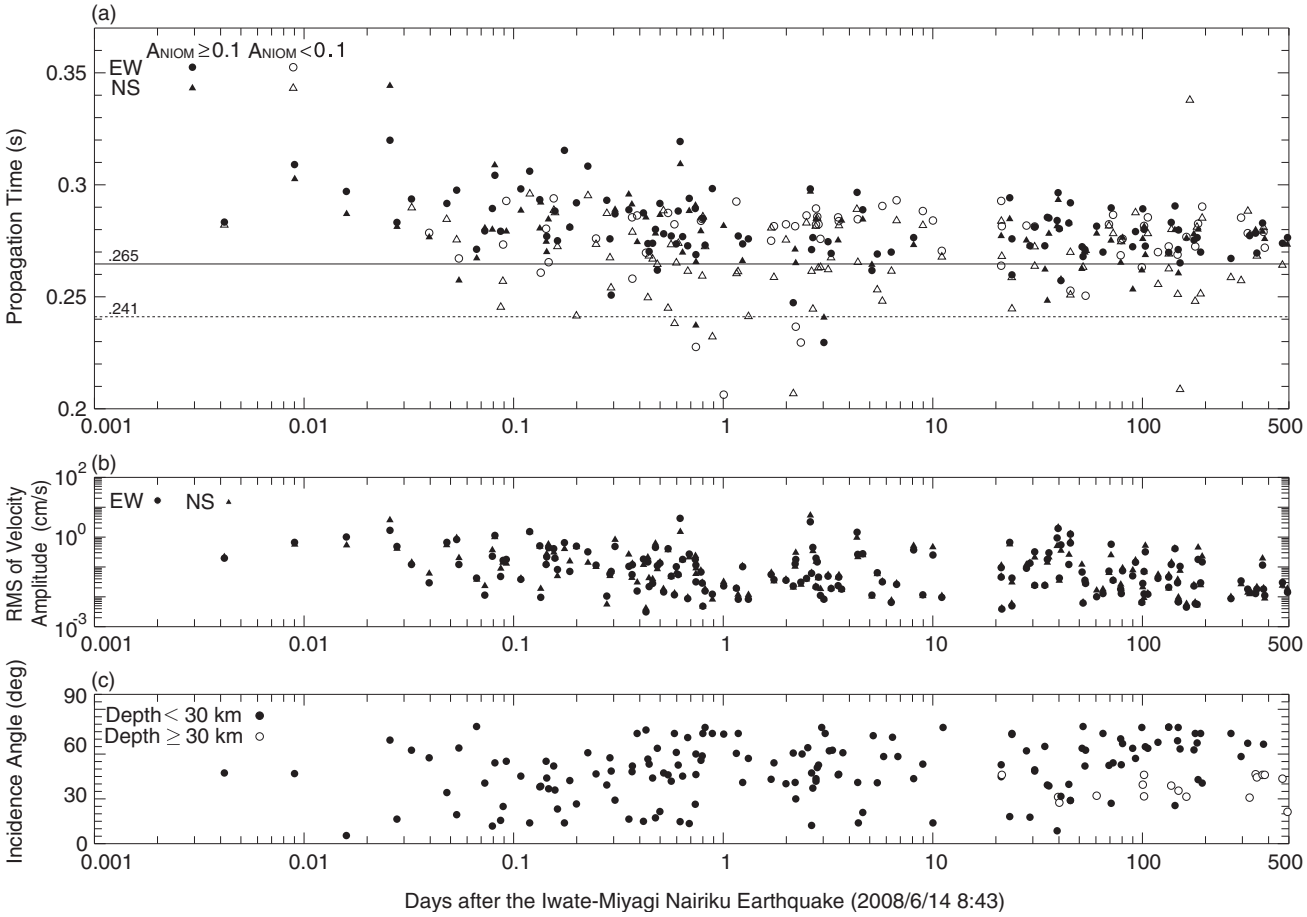

Figure 11. (a) Propagation times (before the vertical corrections) obtained from the events after the 2008 Iwate-Miyagi Nairiku earthquake. (b) RMS values of the velocity amplitudes during each time window. (c) Incidence angles of direct S waves theoretically estimated by using a horizontally layered ground structure.

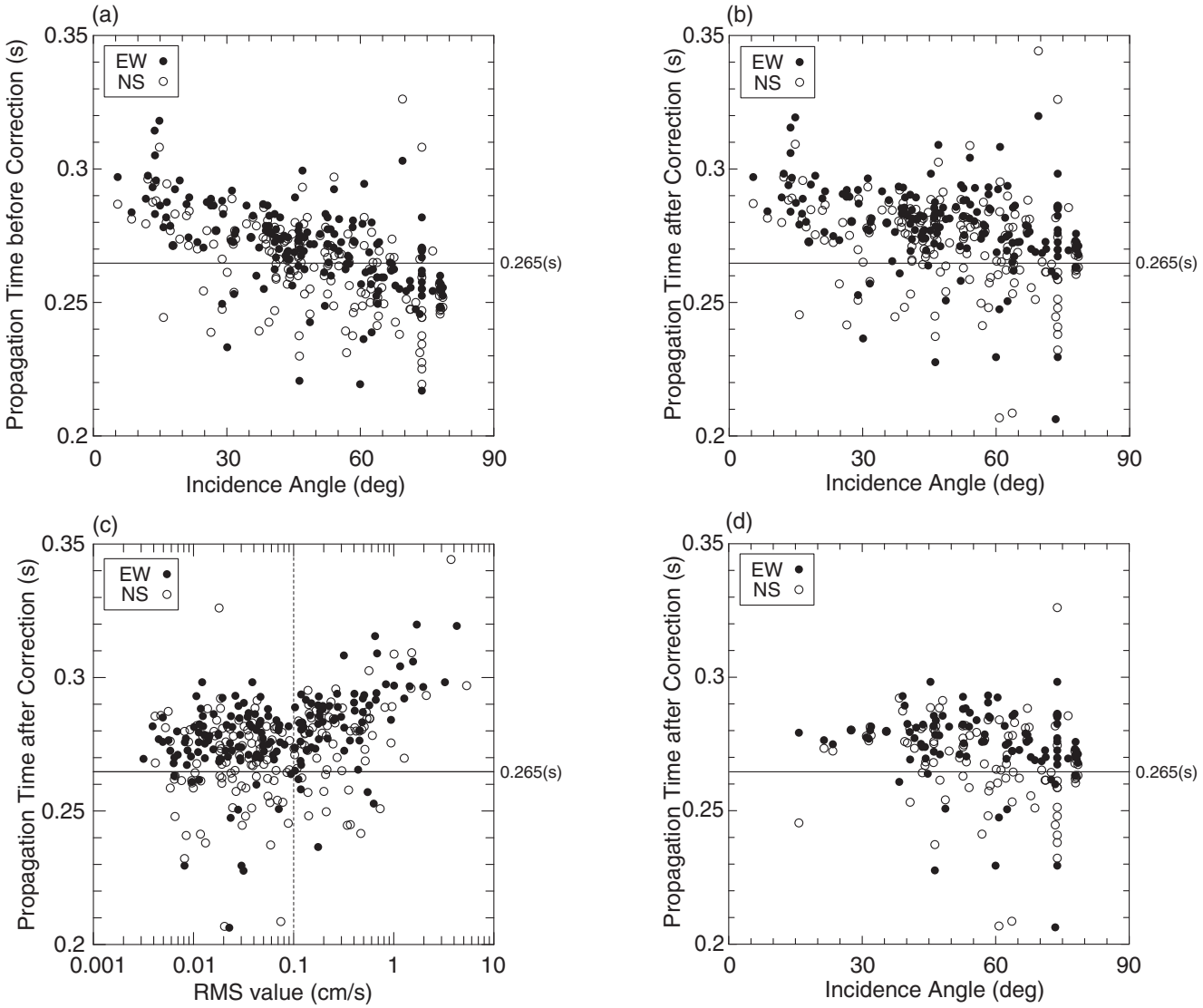

Figure 12. (a) Relationship between incidence angles and uncorrected propagation times observed during the events after the Iwate-Miyagi Nairiku earthquake. (b) Similar relationship to the one shown in diagram (a) but with vertical corrections to the propagation times. (c) Relationship between corrected propagation times and RMS values of the velocity amplitudes. (d) Relationship between corrected propagation times and incidence angles whose RMS values are lower than 0.1 cm/s.

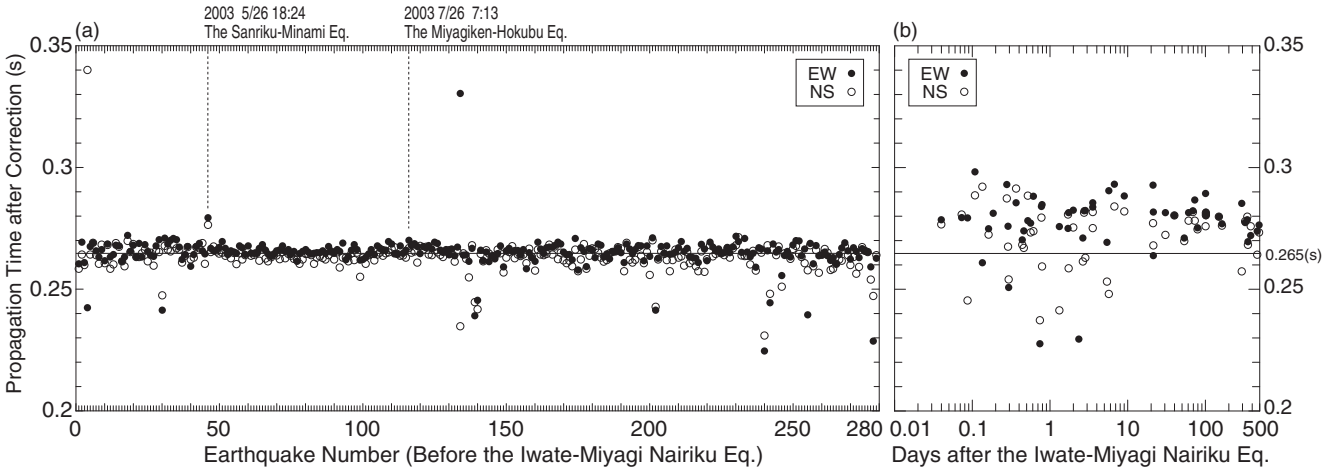

Figure 13. (a) Propagation times of the events before the 2008 Iwate-Miyagi Nairiku earthquake. These are similar to what is shown in Figure 7a but have vertical corrections. (b) Relationship between elapsed days and propagation times. This diagram is analogous to Figure 11a, but includes only results whose RMS values and incidence angles were less than 0.1 cm/s and 60 degrees, respectively.

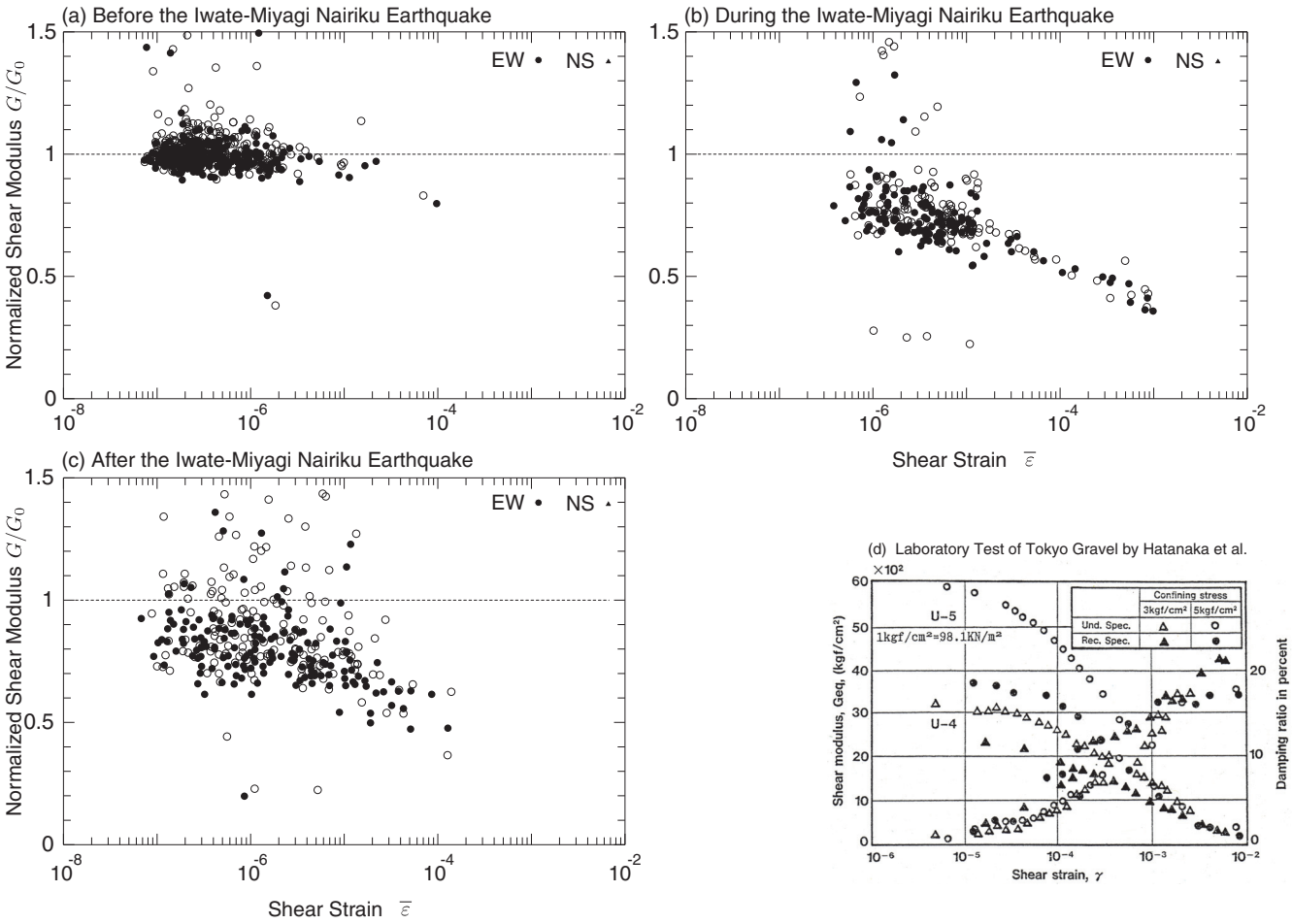

Figure 14. Relationship between shear strains and normalized shear moduli in the second layer obtained from (a) events before, (b) during, and (c) after the mainshock of the 2008 Iwate-Miyagi Nairiku earthquake. For the events before and after the mainshock, the propagation times after vertical corrections were used to evaluate the shear strains and shear moduli. (d) Relationship between shear strains and shear moduli obtained in laboratory tests of undisturbed and reconstituted specimens of Tokyo gravel by Hatanaka et al. (1988) [Reprinted from *Soils and Foundations*, **28**, 4, p. 67, Fig. 13, courtesy of Prof. Hatanaka].